The effect of using nanofluid flow into a porous channel in the CPVT under transient solar heat flux based on energy and exergy analysis

Mahdi Deymi-Dashtebayaz[1] · Mojtaba Rezapour[1]

Abstract

Concentrator photovoltaic thermal system is one of the heat and power generation systems that have received special attention in recent decades. In this paper, concentrator photovoltaic thermal cell with the effect of Al_2O_3 nanofluid flow in porous channel has been investigated under transient heat flux. The system is analyzed from energy and exergy viewpoint, and also the first and second laws of thermodynamics efficiencies are calculated. The governing equations are continuity, Brinkman momentum and energy conservation equations considering the transient solar flux using parabolic dish concentrator over a day in Mashhad city. The numerical modeling is based on the finite element method. The numerical results show that the Nusselt number, normalized temperature and electrical efficiency of the presented model have an acceptable agreement with experimental data. Efficiency of the photovoltaic cell increases with increasing the Reynolds number as the difference between the highest and the lowest efficiency value is 5% at 12 p.m. In addition, with increasing Reynolds number, the first law of thermodynamics efficiency increases due to porosity and permeability effects of the porous channel cooling. The maximum difference between highest and the lowest value for first law efficiency is 49.4% at Re = 110. The second law of thermodynamics efficiency decrease as Reynolds number increases as the highest value is 4.2% and the lowest is 2.8% at Re = 20 and Re = 10, respectively.

Keywords Concentrator photovoltaic thermal · Porous channel · Transient solar heat flux · Photovoltaic cell efficiency

List of symbols

A	Area (m^2)
c_p	Heat capacity ($J\ kg^{-1}\ K^{-1}$)
CR	Concentration ratio
D	Concentrator diameter (m)
f	Focal length (m)
H	Height (mm)
h	Convective heat transfer coefficient ($W\ m^{-2}\ K^{-1}$)
I	Irradiation ($W\ m^{-2}$)
K	Permeability (m^2)
k	Thermal conductivity ($W\ m^{-1}\ K^{-1}$)
L	Length (mm)
$\dot{m}$	Mass flow rate ($gr\ s^{-1}$)
P	Power (w)
P	Pressure ($kg\ m^{-1}\ s^{-2}$)
Q'	Heat flux ($W\ m^{-2}$)
Re	Reynolds number
r	Radius (m)
T	Temperature (K)
t	Time (h)
u	Velocity-x ($m\ s^{-1}$)
v	Velocity-y ($m\ s^{-1}$)
X	Length (m)
Y	Height (m)

Greek symbols

β	Thermal coefficient
ε	Second law efficiency
ε	Porosity
η	First law efficiency
θ	Angel (°)
ρ	Density ($kg\ m^{-3}$)
ρ'	Reflectivity (%)
ϕ	Angel (°)
μ	Dynamic viscosity ($kg\ m^{-1}\ s^{-1}$)
∇	Gradient

Subscripts

Al	Aluminum
amb	Ambient

✉ Mahdi Deymi-Dashtebayaz
mahdi.deymi@gmail.com; m.deimi@hsu.ac.ir

1   Department of Mechanical Engineering, Center
of Computational Energy, Hakim Sabzevari University,
Sabzevar, Iran

CPVT	Concentration photovoltaic thermal
c	Channel
cell	PV cell
eff	Effective
in	Inlet
nf	Nanofluid
out	Outlet
ref	Reference
rim	Rim angel
s	SUN
w	Wall

Introduction

The increasing demand for energy, lack of fossil fuels and their limitations due to the environmental issues caused by pollutants led to the development of renewable energies [1] and energy saving methods [2]. One of the most important and extensive sources of renewable energy is the solar energy [3] which is more accessible than any other renewable energy source [4]. Due to its potentials, different methods suggested to capture the solar energy mainly in the form of heat and electricity. Concentrator photovoltaic thermal (CPVT) is the most widely used equipment in this field capable of supplying both thermal and electrical energy [5]. The efficiency improvement of these collectors can lead to application development of them in such systems.

Various studies have been performed on CPVT numerically [6] and experimentally [7]. One of effective parameters on efficiency of CPVT systems is type of concentrator [8] or photovoltaic cell [9]. In this regard, Shadmehri et al. [10] worked on three-dimensional computational modeling of a new CPVT combined with thermoelectric system and triangular absorber. Finally, they proposed a range for reflector's aperture widths and absorber's apex angles for optimum thermal and electrical performances. Alizadeh et al. [11] simulated a PV cooling by means of the single turn pulsating heat pipe numerically and showed that using a copper fin reduces the temperature of PV panel just 4.9 K. In addition, the pulsating heat pipes cooling increased the power generation up to 18% for 1000 W m^{-2} solar irradiation. Kandilli studied a composite solar photovoltaic hybrid system based on the spectrometric decomposition approach for the introduction, modeling, testing [12] and evaluation of systems [13]. The final results showed that the second law (exergy) efficiency of the concentrator, vacuum tube and overall CPVCS are 12.06%, 2.0% and 1.16%, respectively. Sanaye and Sarrafi [14] conducted exergy and economic analysis over a CCHP solar generation system coupled with conventional photovoltaic, CPVT and evacuated tube (ET) collectors. They found that the maximum exergy efficiency of 29% can be obtained using this model. Ferchichi et al.

[15] developed a numerical model to predict accurately the phase change and the heat transfer in the direct steam generation parabolic using collector system. They reported that an increase in the inlet mass flow rate up to 0.43 kg s^{-1} leads to improving the global thermal efficiency of the collectors by 0.34%. The equations of parabolic dish concentrator (PDC) including various solar collectors and receivers equations can be found in the literature [16].

There are several ways to increase the thermal efficiency of CPVT. One of these ways is to use the nanofluid [17] as a working fluid instead of the conventional fluids [18]. In this regard, Xu and Kleinstreuer [19] designed CPVT systems that can provide both electrical and thermal energies while reducing solar cell material usage via optical techniques. According to their results, the best performance was achieved using a channel with the height of 10 mm and inlet Reynolds number of around 30,000, yielding a modest system efficiency of 20%. Fayaz et al. [20] accomplished a three-dimensional numerical analysis on photovoltaic thermal (PVT) systems using water and multi-walled carbon nanotube-water nanofluid and validated it experimentally. They obtained an overall efficiency improvement of 6.26% numerically and 5.73% experimentally. Eric et al. [21] studied an innovative thermal performance evaluation of a parabolic trough collector operating with green-synthesized nanofluids: water/BH-SiO$_2$ and water/OLE-TiO$_2$. They developed the model of the parabolic trough collector (PTC) and the results showed that a 0.073% mean enhancement in the thermal efficiency is observed with the use of water/BH-SiO$_2$ nanofluids and 0.077% mean enhancement is achieved with the use of water/OLE-TiO$_2$ nanofluids. An et al. [22] developed and experimentally validated a model to predict the performance of high-temperature nanofluid-based spectral splitting PVT systems for a wide range of optical properties, flow rates and solar concentration ratios. Mousa et al. [23] conducted a systematic comparison solar system for industrial applications based on their cost, performance and environmental impact globally. Fanaee and Rezapour [24] analyzed thermal-fluid modeling of non-porous/porous thermal coil filled by alumina nanofluid considering constant/variable solar heat fluxes. Radwan et al. [25] used Al$_2$O$_3$-water and SiC-water nanofluids with different volumetric ratios for a new cooling technique in low concentrated photovoltaic–thermal (LCPV/T) systems. Alobaida et al. [26] investigated to evaluate the recent advances in the field of solar absorption cooling systems from solar collector types. A review in the area of photovoltaic thermal (PVT) absorption cooling systems is provided in their work. Ragab et al. [27] worked experimentally on utilization of the nanofluid as a working agent for PVT. The best system efficiencies were obtained at 0.075% V of multi-walls carbon nanotubes—water-based nanofluid. Hader and Kouz [28] evaluated the innovative hybrid solar panels combining

photovoltaic cells along with an efficient heat exchanger with the fins attached to the parallel plates using water-Al_2O_3 nanofluid as the working fluid. Their results showed that when the Reynolds number, the length of the fin and the volume fraction of the nanosolid particles increase, the overall efficiency increases.

The structure of the porous media can also be effective in increasing the thermal efficiency. Many researches have been done to investigate the flow of fluids or nanofluids in porous media. One of the most important outcomes of such researches is the increase in Nusselt number and consequently the increase in heat transfer [29–38]. Furman et al. [31] proposed a simple foam structure model based on the interaction between sodium chloride solid particles poorly wetted by melted aluminum, which leads to the formation of air pockets (or "air collars"), for the permeability of porous material. Dukhan and Chen [34] analyzed flow and heat transfer of air into aluminum metal foams under constant heat flux experimentally and numerically and described the dimensionless temperature profiles. Anoop et al. [35] investigated experimentally heat transfer characteristics in the tube with constant heat flux with Al_2O_3 nanofluids. Xu and Zhao [36] investigated fully developed forced convective heat transfer in porous medium subject to asymmetrical heating with different models analytically. The classic Darcy and Brinkman models were employed for the fluid flow, while the local thermal equilibrium and the local thermal non-equilibrium models were employed to describe the heat transfer process in porous media. Open-cell metal foam is experimentally investigated as a flow field for a new bipolar plate design by Awin and Dukhan [37]. Chen et al. [38] investigated the heat transfer characteristics of a double-pipe heat exchanger with metal foam insert numerically. Their resulted for the designs of graded foam structure, using lower porosity and small pore density at both side of the inner pipe wall shows better overall performance with the performance factors of 4.41 and 4.54. Ghahremannezhad and Vafai [39] designed a microchannel heat sink (MCHS) which improves thermal and hydraulic performance of conventional microchannels. They analyzed three-dimensional models of MCHS with different solid and porous fin thicknesses. In Ref. [40], various forms of fluid equations in a porous medium, as an embedment of Navier–Stokes equation, are discussed for the single-phase flow. Bellos and Tzivanidis [41] investigated a thermal photovoltaic system with and without nanofluids. The used nanofluid was based on copper oxide which is able to operate at an inlet temperature of 200 °C. The most important result of this study was the increase in thermal and electrical efficiency by 46.84% and 6.60%, respectively. Gu et al. [42] performed the economic and technical evaluation on a solar photovoltaic system intended for use in buildings in Sweden using optical analysis based on the Monte Carlo method assuming eleven

basic input variables. It was ultimately concluded that their studied photovoltaic system would be profitable. In another work, Bellos et al. [43] also discussed the use of a decentralized thermal photovoltaic system in a heat pump for use in a residential home. Their results showed that using this system increased energy and exergy efficiency by 4.80% and 0.66%, respectively.

The literature survey shows that significant works have been done on increasing the efficiency through employing nanofluids or focused on increasing the heat transfer and power generation by using porous media. However, not much focus has been given to the simultaneous use of nanofluids and porous media and its effect on performance of the system.

In addition, most of the previous studies have not much addressed the influence of time variable solar heat flux. In this paper, the performance of a solar thermal photovoltaic system using Al_2O_3 nanofluid flowing into the porous channel is analyzed during a day in Mashhad city of Iran. The effects of the nanofluid flow in porous channel on the photovoltaic cell temperature and PV cell efficiency under the time variable solar heat flux and also the heat flux received from the parabolic dish concentrator are discussed. Finally, the system is evaluated from the energy and exergy viewpoints and the first and second laws of thermodynamics efficiencies are calculated. The investigation of the PV cell efficiency, temperature of nanofluid and PV cell and also energy and exergy analysis of PV cell, porous channel are the most important achievements in this work.

Model description

A schematic view of the photovoltaic thermal cell with PDC is shown in Fig. 1. The system is designed to provide both thermal and electrical energies using thermal porous collector and photovoltaic cells. The solar heat fluxes are received by concentrator and photovoltaic cell are equal to I and q'', respectively. The concentrator is positioned in a direction perpendicular to the solar irradiation and is made of aluminum with a reflectance coefficient ρ'. Furthermore, the study is performed in Mashhad city with latitude and longitude coordinates of 37.27 and 59.63 located in the northeast of Iran for a sunny day in summer (July 15). The amount of solar irradiation reaches the concentrator and the top of the photovoltaic cell within 24 h is equal to I, while the amount of solar heat flux concentrated on bottom of the photovoltaic cell by concentrator is equal to Q'. Accordingly, I is used for heat flux related to the top of the PV cell and Q' is used for heat flux related to the bottom of the PV cell. In addition, the input energy and exergy are obtained based on I and Q' used in some equations.

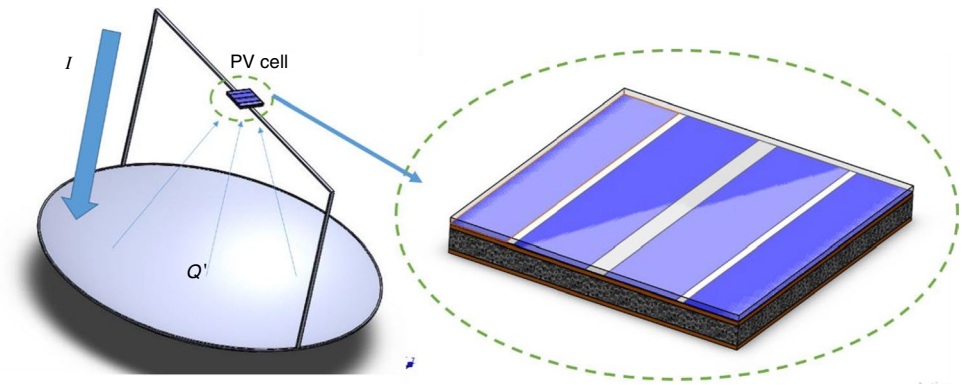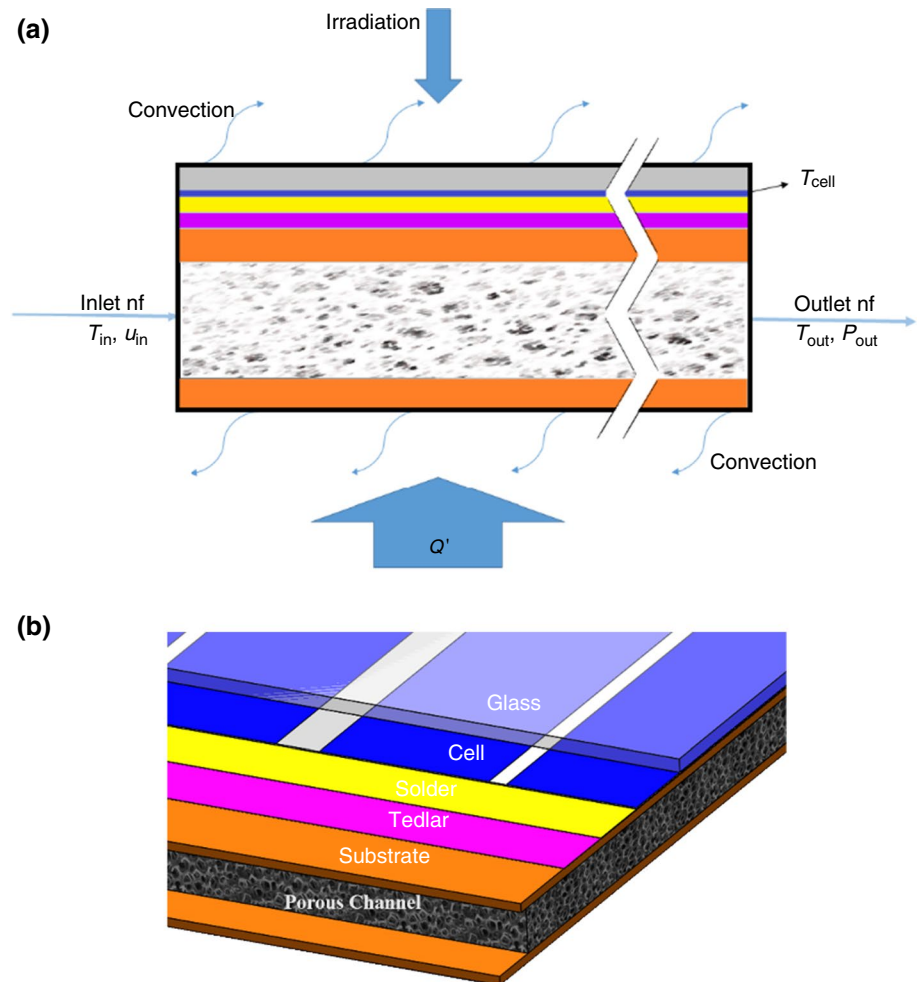**Fig. 1** The schematic view of the model

Fig. 2 **A** The boundary condition of the model. **b** The layers of photovoltaic thermal cell

The photovoltaic thermal system consists of some layers with boundary conditions shown in Fig. 2. The length of this system is proportional to the dimensions of photovoltaic cell which is L and its height is equal to H which is considered based on the channel. The selected metal porous foam is composed of aluminum material with porosity of ε and permeability of K. The inlet temperature of the collector, local temperature of nanofluid, the temperature of photovoltaic cell and the output pressure of the solar collector are T_{in},

T_{nf} is T_{cell} and P_{out}, respectively. The flow in the porous collector is analyzed with the Brinkman equation considering Reynolds number limited between 10 and 120.

The two-dimensional view of the parabolic dish concentrator with the most important geometrical parameters are shown in Fig. 3a. As shown in this figure, D is Concentrator diameter and h, ρ, f, $\varnothing_{rim}$ represent height of curve, radius, focal length and rim angle, respectively. The concentrator is made with aluminum. Figure 3 shows various finite
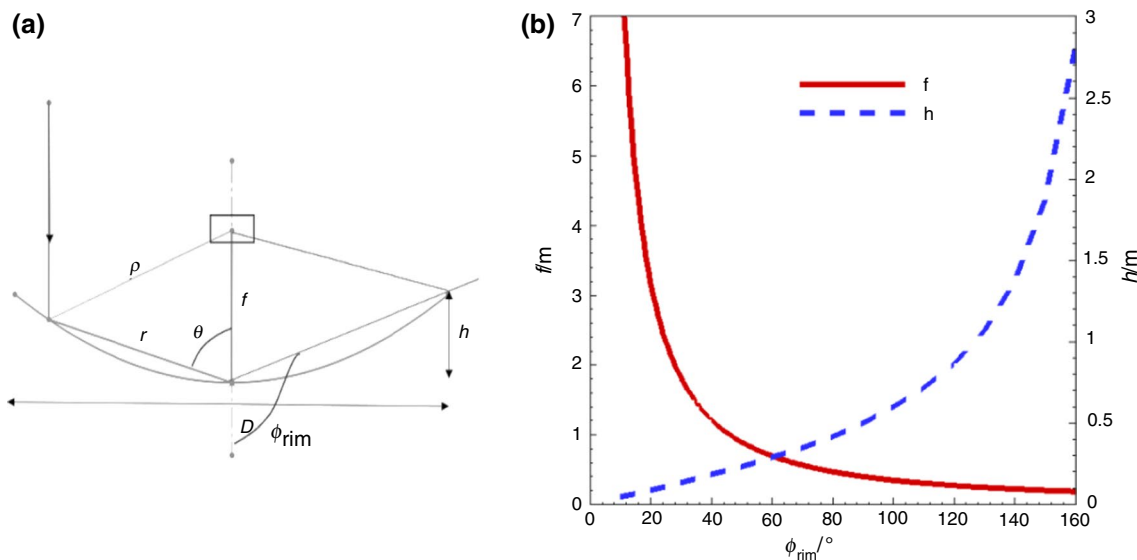
Fig. 3 **a** The 2D schematic view of solar parabolic dish concentrator. **b** The variation of focal length and height of concentrator versus rim angle

parabola curves having a common focus and the same aperture diameter.

The numerical model is based on two-dimensional unsteady state condition where $L = 156$ mm, $H = 10$ mm and PV cell dimensions are according to LG305N1C-B3 PV Cell [44]. The characteristics of the coupled system are selected as $\varepsilon = 79.6\%$, $d_p = 5 \times 10^{-4}$ and $T_{in} = 300$ K. For the concentrator, $D = 2$ m, $\emptyset_{rim} = 30°$ and the reflectivity is equal to 92%.

Governing equation

The equations used for nanofluid properties are same as those used in our previous work [24]. In order to analyze the fluid flow into a two-dimensional channel, the governing equations including continuity and momentum (Brinkman's equation) are employed:

$$\frac{\partial u}{\partial t} + \frac{\partial u}{\partial u} + \frac{\partial v}{\partial y} = 0 \tag{1}$$

$$\frac{\rho_{nf}}{\varepsilon^2}\left(\frac{\partial u}{\partial t} + u\frac{\partial u}{\partial x} + v\frac{\partial u}{\partial y}\right) = -\frac{\partial p}{\partial x} + \frac{\mu_{nf}}{\varepsilon}\left(\left(\frac{\partial^2 u}{\partial x^2} + \frac{\partial^2 u}{\partial y^2}\right) + \frac{2}{3}\left(\frac{\partial u}{\partial x} + \frac{\partial u}{\partial y}\right)\right) - \frac{\mu_{nf}}{K}u \tag{2.1}$$

$$\frac{\rho_{nf}}{\varepsilon^2}\left(\frac{\partial v}{\partial t} + u\frac{\partial v}{\partial x} + v\frac{\partial v}{\partial y}\right) = -\frac{\partial p}{\partial y} + \frac{\mu_{nf}}{\varepsilon}\left(\left(\frac{\partial^2 v}{\partial x^2} + \frac{\partial^2 v}{\partial y^2}\right) + \frac{2}{3}\left(\frac{\partial v}{\partial x} + \frac{\partial v}{\partial y}\right)\right) - \frac{\mu_{nf}}{K}v \tag{2.2}$$

In Eqs. 2.1 and 2.2, K represents the permeability tensor of the porous channel. As presented in Eq. 3, it is a function of the porosity and diameter of porous media holes for an isotropic porous medium [40].

$$K = \frac{D_p^2 \varepsilon^3}{a(1 - \varepsilon)^2} \tag{3}$$

This equation is expressed in terms of Carmen's theory where a is a constant equal to 180 [40]. In addition, the energy equation is as follow:

$$\rho C_p\left(\frac{\partial T}{\partial t} + u\frac{\partial T}{\partial x} + v\frac{\partial T}{\partial y}\right) = k\left(\frac{\partial^2 T}{\partial x^2} + \frac{\partial^2 T}{\partial y^2}\right) + Q \tag{4}$$

It should be noted that in above equations, u represents the Darcy velocity in the porous medium obtained from Eq. (5):

$$\vec{u} = \varepsilon\vec{u} \tag{5}$$

The value of k_{eff} for porous collector is related to thermal conductivity of fluid and porous particle as [30, 40]:

$$k_{\text{eff}} = k_{\text{Al}}\varepsilon + k(1 - \varepsilon) \tag{6}$$

Moreover, the average fluid temperature in the collector is calculated as follow [28]:

$$T_{\text{m}}(x) = \frac{\int_0^H uT\mathrm{d}y}{\int_0^H u\mathrm{d}y} \tag{7}$$

In this study, the parabolic dish concentrator is used and an parabolic equation is used for the concentrator [16]:

$$x^2 = 4fy \tag{8}$$

According to geometrical parameters of parabolic dish concentrator shown in Fig. 3, the relation between focal length with rim angle and r is as follow [16]:

$$\frac{\sin^2 \theta}{\cos \theta} = \frac{4f}{r} \tag{9}$$

$$\rho = \frac{2f}{1 + \cos \phi_{\text{rim}}} \tag{10}$$

In terms of focal length and aperture diameter, for the parabolic dish concentrator with a small rim angle, the height of the parabola is [16]:

$$h = \frac{D^2}{16f} \tag{11}$$

Also, the relation between rim angle and focal length with concentrator diameter is [16]:

$$\frac{f}{D} = 1 / \left(4 \tan \frac{\phi_{\text{rim}}}{2} \right) \tag{12}$$

Furthermore, reflected flux of parabolic concentrator is achieved according to following equation [12, 13]:

$$Q' = \pi f^2 \frac{1}{2} \left[(1 - \cos(2\phi_{\text{rim}})) - (1 - \cos(2\phi_{\text{s}})) \right] \rho' I \tag{13}$$

In above equation, ϕ_s is shadow angle that is calculated from following equation [16]:

$$\phi_{\text{s}} = \tan^{-1}(D_{\text{c}}/f) \tag{14}$$

If the equivalent diameter of the porous collector D_{c} is much smaller than the focal length, the shadow angle will be zero.

The convective heat transfer from top and down shown in Fig. 2a can be defined as follow:

$$Q_{\text{c}} = h(T_{\text{b}} - T_{\text{amb}}) \tag{15}$$

The thermal energy received from the porous channel is obtained from Eq. 16:

$$\dot{q}_{\text{c}} = \dot{m}C(T_{\text{out}} - T_{\text{in}}) \tag{16}$$

The exergy of photovoltaic cell, exergy of porous channel and the maximum efficiency ratio Ψ for the exergy from the sun can be found by the Petela's formula from the following equations, respectively [12, 13]:

$$\phi_{\text{c}} = \dot{m}C\left[(T_{\text{out}} - T_{\text{in}}) - T_{\text{amb}}\left(Ln\frac{T_{\text{out}}}{T_{\text{in}}} \right) \right] \tag{17}$$

$$\phi_{\text{cell}} = \eta_{\text{cell}}IA_{\text{cell}} \tag{18}$$

$$\psi = 1 + \frac{1}{3}\left(\frac{T_{\text{amb}}}{T_{\text{s}}} \right)^4 - \frac{4}{3}\frac{T_{\text{amb}}}{T_{\text{s}}} \tag{19}$$

In Eq. (19), the solar temperature is 6000 K. The thermal efficiency for the channel equals to the ratio of the energy received from the channel to the total energy received from the sun and the concentrator is as follows [13]:

$$\eta_{\text{c}} = \frac{\dot{m}C(T_{\text{out}} - T_{\text{in}})}{A_{\text{cell}}(Q' + I)} \tag{20}$$

The efficiency of the photovoltaic cell is equal to the following relation [19]:

$$\eta_{\text{cell}} = \eta_{\text{ref}}[1 - \beta(T_{\text{cell}} - T_{\text{ref}})] \tag{21}$$

The first law efficiency and the second law efficiency for a thermal photovoltaic system for thermal photovoltaic system are [12, 13]:

$$\eta_{\text{cpvt}} = \frac{\eta_{\text{cell}}I + \dot{m}C(T_{\text{out}} - T_{\text{in}})}{A_{\text{c}}I} \tag{22}$$

$$\varepsilon_{\text{cpvt}} = \frac{\phi_{\text{cell}} + \phi_{\text{c}}}{\phi_{\text{in}}} \tag{23}$$

where the β is a constant value and the Reynolds number is calculated using Eq. 24 which is in terms of density, hydraulic diameter and viscosity of nanofluid.

$$Re = \frac{\rho_{\text{nf}}u_{\text{nf}}D_{\text{h}}}{\mu_{\text{nf}}} \tag{24}$$

In this respect, the hydraulic diameter of the porous channel is equal to the following relationship:

$$D_{\text{h}} = \frac{4A_{\text{in}}}{P_{\text{in}}} \tag{25}$$

The concentration ratio is considered based on PV cell area and concentration area as follow:

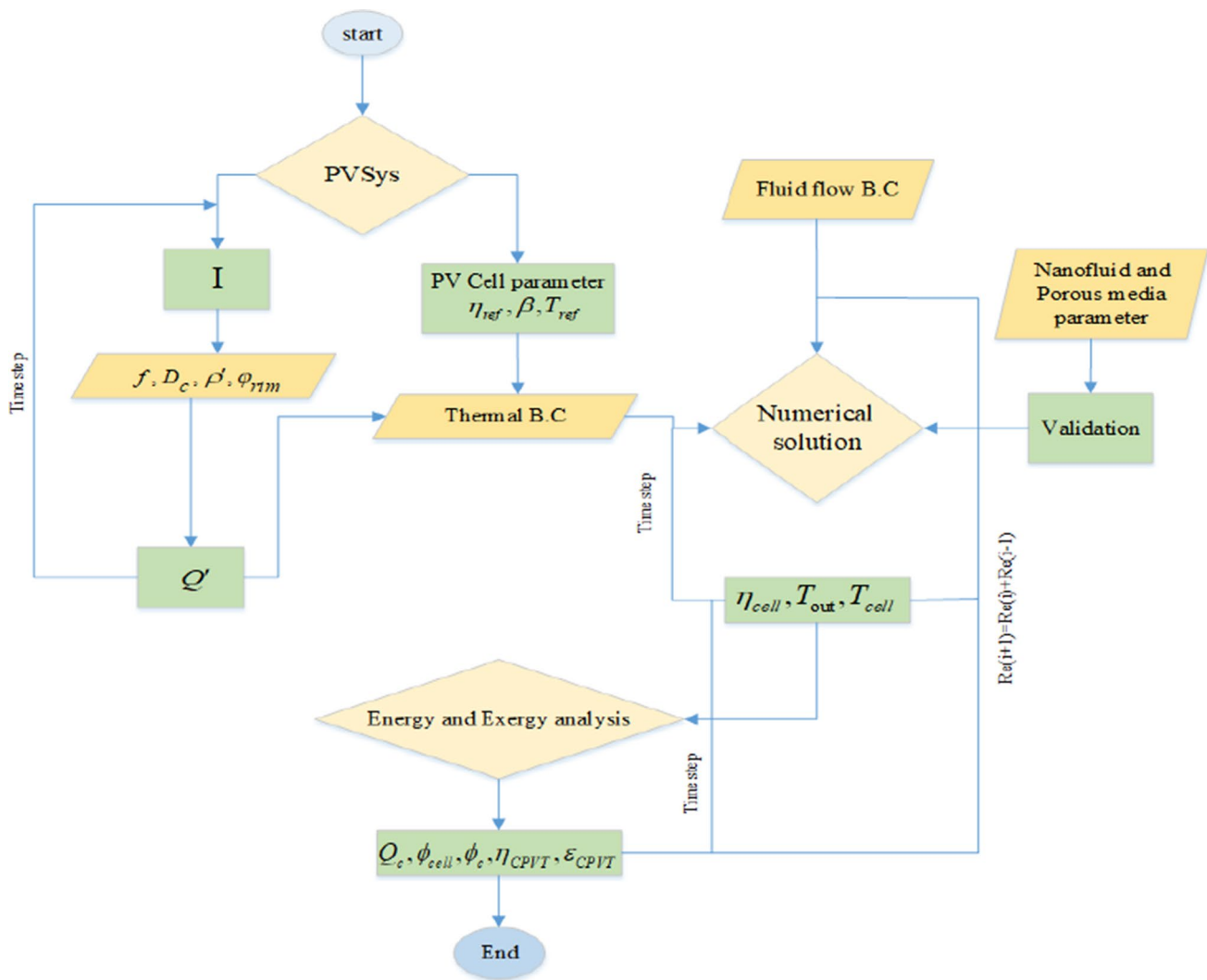**Fig. 4** The diagram of solution method for present model

$$CR = \frac{A_C}{A_{Cell}} \qquad (26)$$

The optical efficiency is defined as a function of solar heat fluxes, concentrator area and PV cell area:

$$\eta_{opt} = \frac{Q' A_{cell}}{I A_C} \qquad (27)$$

The time variable solar heat flux and photovoltaic cell information were obtained from PVSys software and used for the numerical solution of the nanofluid flow in the porous channel. The numerical solution method is based on the finite element and direct method of MUMPS[1] solver. Then,

the thermodynamic analysis of the system is conducted based on the energy and exergy by calculating the thermal parameters according to computational fluid dynamics solution. The diagram of the solution method is shown in Fig. 4.

Result

In this paper, the use of a solar thermal photovoltaic system coupled with Al_2O_3 nanofluid flow into the porous channel is investigated over a day for Mashhad city in Iran. The numerical model is based on two-dimensional unsteady-state condition. The result in this section consists of three sections which is discussed in detail.

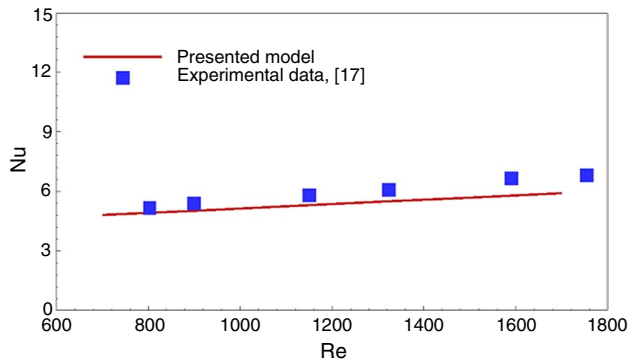[1] Multi-frontal massively parallel sparse direct solver.

Fig. 5 The comparison between variation of Nusselt number at the present model and experimental data [17] for 4% of nanofluid into a non-porous collector at $x/D = 147$
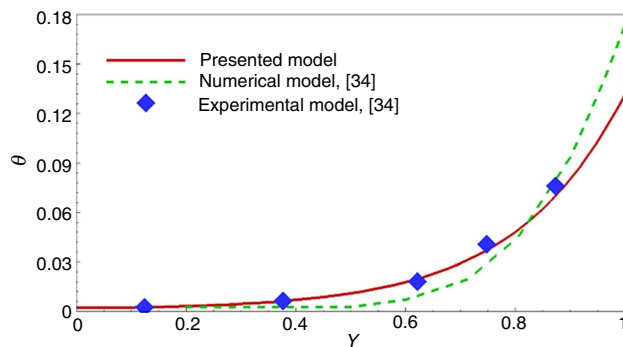

Fig. 6 The comparison between variation of normalized temperature versus height of foam for present model and experimental data and numerical results [34] with $\varepsilon = 79.6\%$

Validation

For validation of the model, the Nusselt number in non-porous media is firstly investigated for acceptable Al_2O_3 properties. Then, the dimensionless temperature in porous media is analyzed for fluid flow and heat transfer in porous medium. Finally, the electrical efficiency of PV cell with nanofluid flow without porous media is evaluated. The Nusselt number is initially checked to investigate the accuracy of the result obtained for nanofluid flow and its properties in a non-porous collector. This validation result is shown in Fig. 5 where the Nusselt number is compared with experimental data for 4% of nanofluid. As seen, the maximum errors between the presented model results and experimental data [17] are equal to 10.8%.

In order to validate the porous medium solution, the values of normalized temperature θ in perpendicular direction obtained from presented model are compared with the numerical and experimental data published in the previous works [34], for aluminum foam with porosity of 79.6% (Fig. 6). According to Fig. 6, the modeling results have an
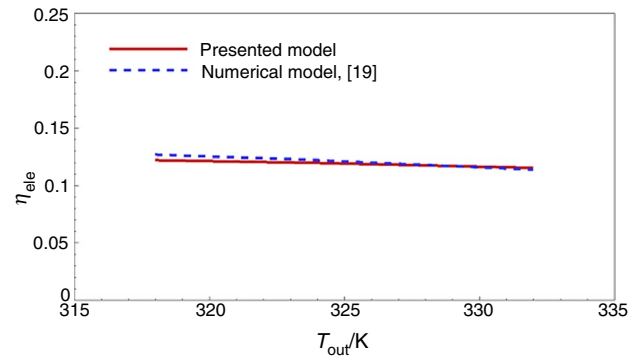

Fig. 7 The comparison between electrical efficiency achieved at the presented model with numerical model [19], for alumina nanofluid

acceptable agreement with the experimental data with maximum errors of 3%. Furthermore, the presented results are closer to the numerical data than to the experimental data.

The electrical efficiency is calculated and shown in Fig. 7 based on the similar conditions selected in the previous work [19]. In this comparison, the nanofluid flow without using porous collector is used. As shown in Fig. 7, the presented data have an acceptable agreement with numerical model [19] with errors of 4%. This difference decreases with decreasing the inlet velocity which is corresponding to increasing the outlet temperature.

Thermal results

Figure 8a shows the variation of solar irradiation I on July 15 for Mashhad city. In addition, the variation of heat flux received by the concentrator Q' on this day are also shown proportional to its solar flux. According to Fig. 8a, the maximum solar irradiation at 12 p.m. equals to 1000 W m^{-2} and the maximum heat flux received by the concentrator is 8500 W m^{-2}. The exergy of the irradiation and the heat flux received by the concentrator during 24 h is shown in Fig. 8b. As shown in this figure, the maximum exergy of the concentrator is when more solar radiation is received by the cell from the concentrator.

Figure 9 shows the variation of the nanofluid temperature of porous channel according to Eq. 7 at different Reynolds number for one day under the influence of solar irradiation and the heat flux received by the concentrator. As the channel length increases, the nanofluid temperature increases. These temperature changes are influenced by the porosity and permeability parameters and the heat which is due to the solar flux and the flux received by the concentrator to the porous channel. Moreover, as the Reynolds number increases, the nanofluid temperature decreases. The rate of nanofluid temperature change is 53.4% at 12 p.m. and
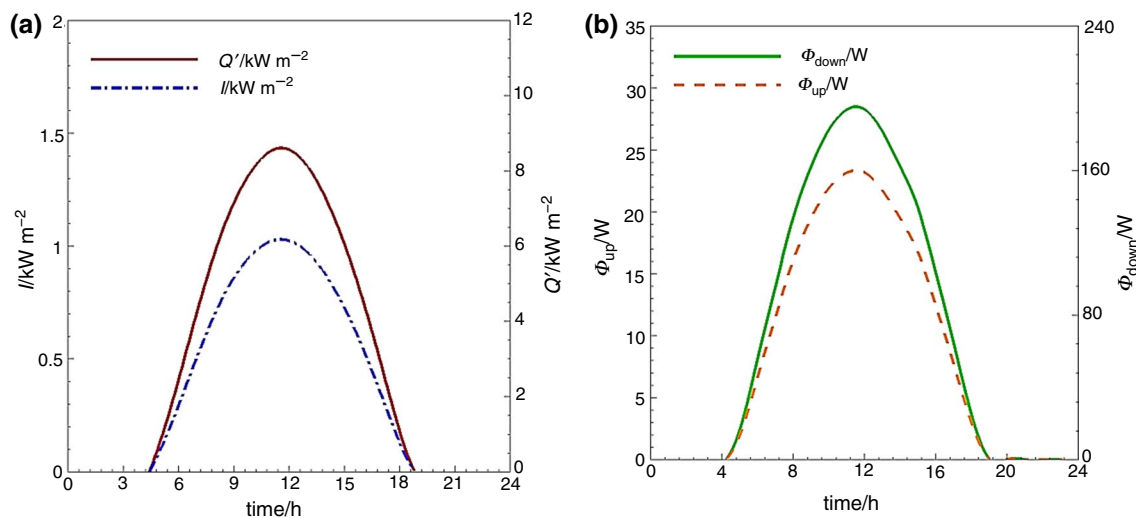
Fig. 8 **a** The variation of solar irradiation and heat flux received from concentrator. **b** The variation of exergy of solar irradiation and heat flux received from concentrator on July 15 for Mashhad city

Reynolds number of 10, while it is 15% at the same time (12 p.m.) and Reynolds number of 110.

In Fig. 10a, the variation of the average outlet temperature of nanofluid in the porous channel is shown at different times of the day and different Reynolds numbers. The highest average nanofluid temperature is 58 °C at Reynolds number of 10, while that it is equal to 32 °C at Reynolds number of 110. In addition, the variation of average outlet temperature of the nanofluid in the porous channel in terms of Reynolds number changes is shown in Fig. 10b. The outlet temperature of nanofluid decreases with increasing the Reynolds number, and the maximum difference of the average outlet temperatures is 26% for 12 p.m. and 16 pm.

The variation of average PV cell temperature over a day for different Reynolds numbers is shown in Fig. 11a. As the Reynolds number increases, the average PV cell temperature decreases at all times of the day. The highest average cell temperature is at 12 p.m. with the highest solar radiation. However, a photovoltaic cell without a porous channel can have a greater temperature at maximum radiation and Reynolds number of 10. Furthermore, the porous channel can have thermal energy and also can reduce the average PV cell temperature. The highest average PV cell temperature is 47 °C at 12 p.m., while at this time, the lowest average PV cell temperature is 30 °C. In Fig. 11b, for the three time periods between 8 a.m. to 16 p.m., the variation of average PV cell temperature is demonstrated versus the Reynolds number. The rate of change is similar with increasing the Reynolds number, while the PV cell temperature change for Reynolds numbers less than 40 is more significant compared to Reynolds numbers greater than 80.

Thermodynamics results

Figure 12a shows the thermal energy received from the porous channel during the day. The maximum amount of thermal energy received from the channel is the maximum during the time when the solar radiation is 215 W at Reynolds number of 110. This result shows that both of the thermal power and the electrical power can be obtained from the porous channel and PV cell. In addition, the thermal power changes versus Reynolds number at three specified times in the morning, noon and evening are shown in Fig. 12b which indicates that the variation of heat energy becomes more uniform at Reynolds numbers greater than 70.

The first law of thermodynamics efficiency of the CPVT is shown in Fig. 13. As shown in this figure, with increasing Reynolds number, the first law efficiency increases (due to porous channel cooling). The highest first law efficiency is 9.5% and the lowest is 2.4%.

Figure 14a shows the variation of PV cell efficiency at different Reynolds numbers. In ideal condition, the PV cell efficiency is 0.2 which is under heat flux of 1000 W m^{-2} and PV cell temperature of 25 °C. As can be seen in Fig. 14a, by increasing the solar heat flux and also the heat flux received from the concentrator the efficiency of the cell decreases but the nanofluid flow inside the porous channel causes less change in cell temperature. Consequently, the PV cell efficiency increases. The increase in PV cell efficiency with increasing Reynolds number is due to the more cooling of the nanofluid flow inside the porous channel. The difference between the highest efficiency and its lowest value is 5% at 12 p.m. It is also seen in Fig. 14b that the effect of flow on PV cell efficiency at Reynolds numbers greater than 70 is much lower than its effect at Reynolds numbers less than 40.
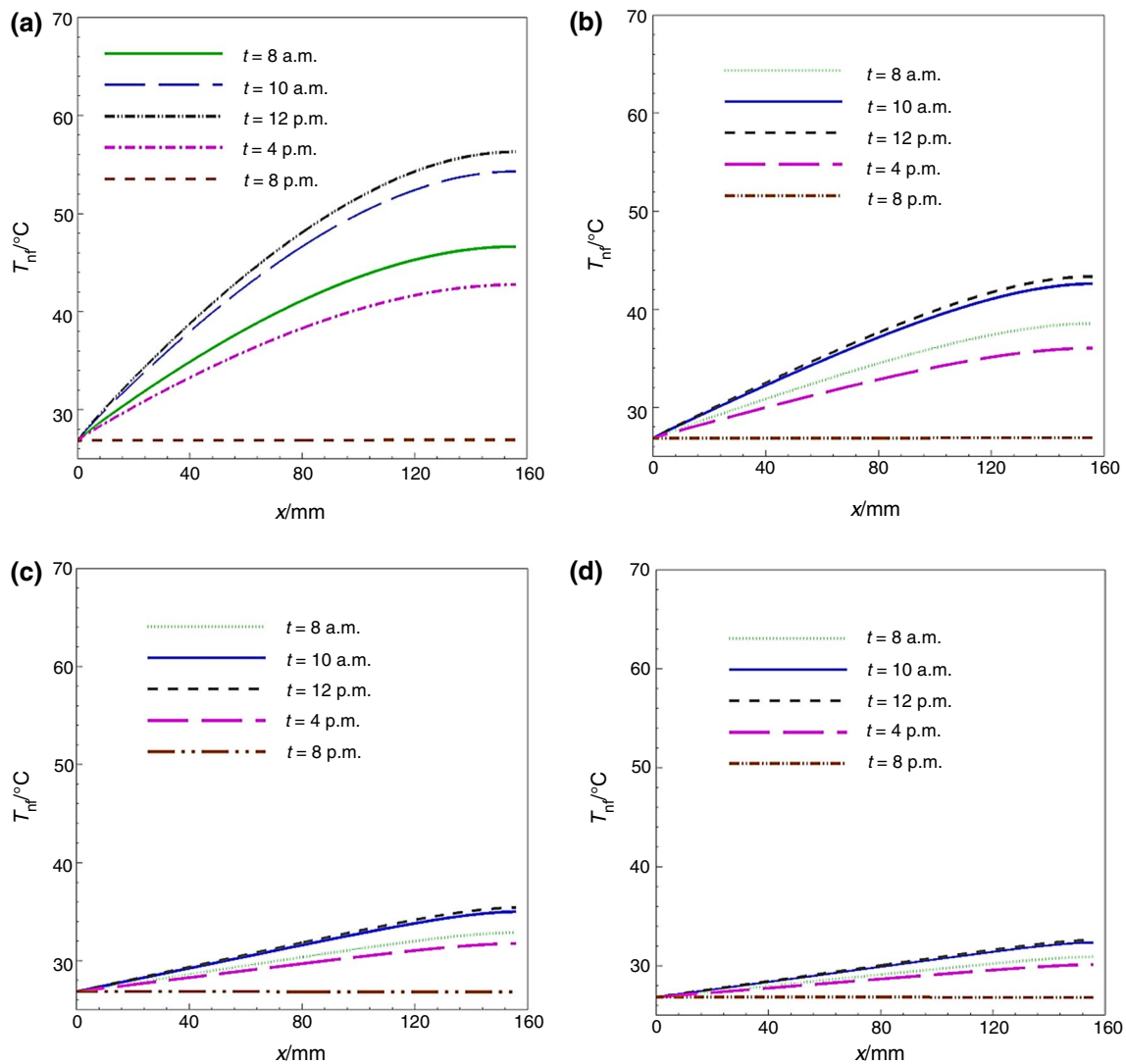
Fig. 9 The variation of the nanofluid temperature of porous channel at different Reynolds, **a** Re = 10, **b** Re = 30, **c** Re = 70 and **d** Re = 110 over a day

The exergy of porous channel and PV cell versus Reynolds number in the morning, noon and evening are shown in Fig. 15a, b, respectively. The variation of exergy of PV cell respect to Reynolds number is small which is due to the low efficiency of the photovoltaic cell as a result of the effects of the flow induced by the porous channel. As shown in Fig. 16a, the increase in Reynolds number is proportional to the decrease in porous channel exergy.

The efficiency of the second law of thermodynamics for the CPVT is shown in Fig. 16. As shown in this figure, the second law of thermodynamics efficiency decreases as Reynolds number increases. The highest second law of thermodynamics efficiency is 4.2% at 12 p.m. and Reynolds number of 20 while the lowest is 2.8%. For all Reynolds

numbers, the exergy efficiency at 12 p.m. is higher than the other hours of the day, as shown in Fig. 16. However, according to Eq. (23), the electrical efficiency decreases as the temperature increases at 12 p.m., but it is more efficient in terms of heat generation and exergy efficiency. The CPVT systems show that the supply of thermal and electric energy can increase exergy efficiency and simultaneously.

In this paper, due to the simultaneous use of porous media and nanofluid, it is possible that the cell temperature does not increase too much which helps to further increase in the electrical efficiency of the cell. On the other hand, thermal energy can also be received from porous channel. Therefore, for these reasons, the proposed system is more efficient
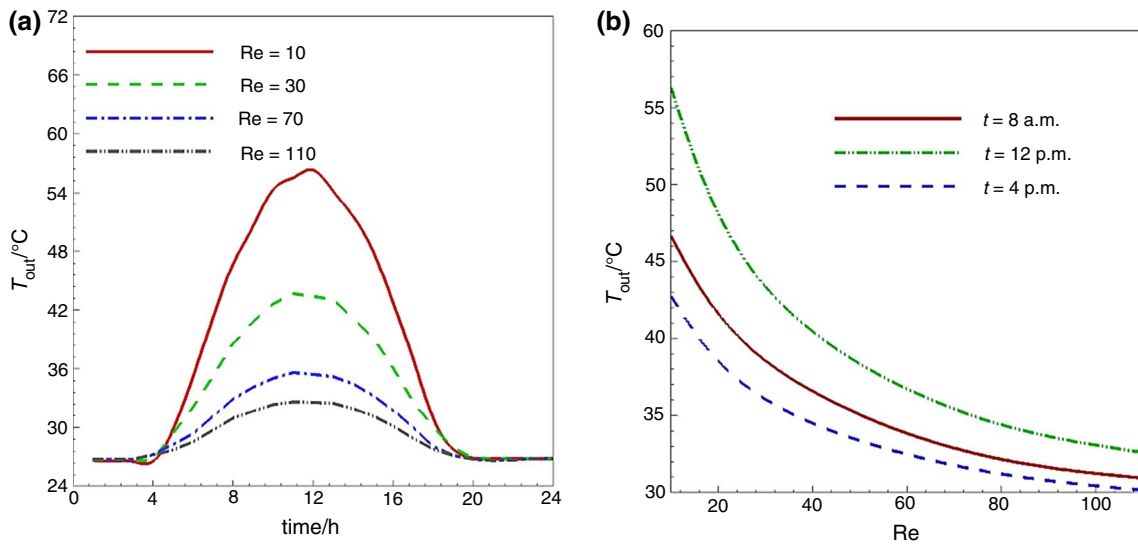
Fig. 10 **a** The variation of the average outlet temperature of nanofluid the porous channel versus time; **b** the variation of average outlet temperature of the nanofluid in the porous channel versus Reynolds
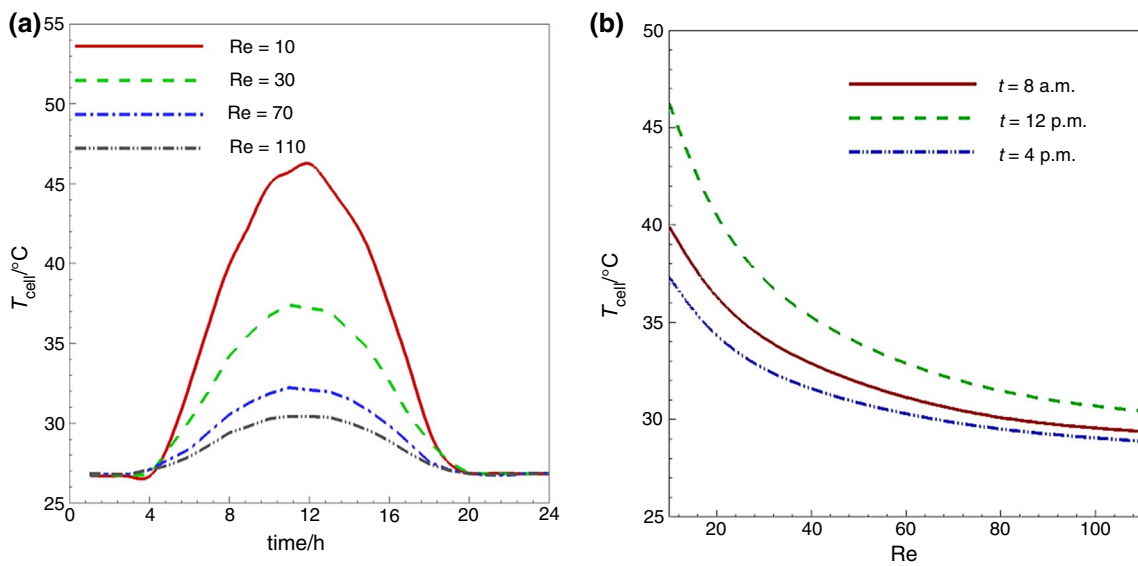

Fig. 11 **a** The variation of average PV cell temperature versus time over a day for different Reynolds. **b** The variation of average PV cell temperature versus Reynolds number at 8 a.m., 12 p.m. and 16 p.m
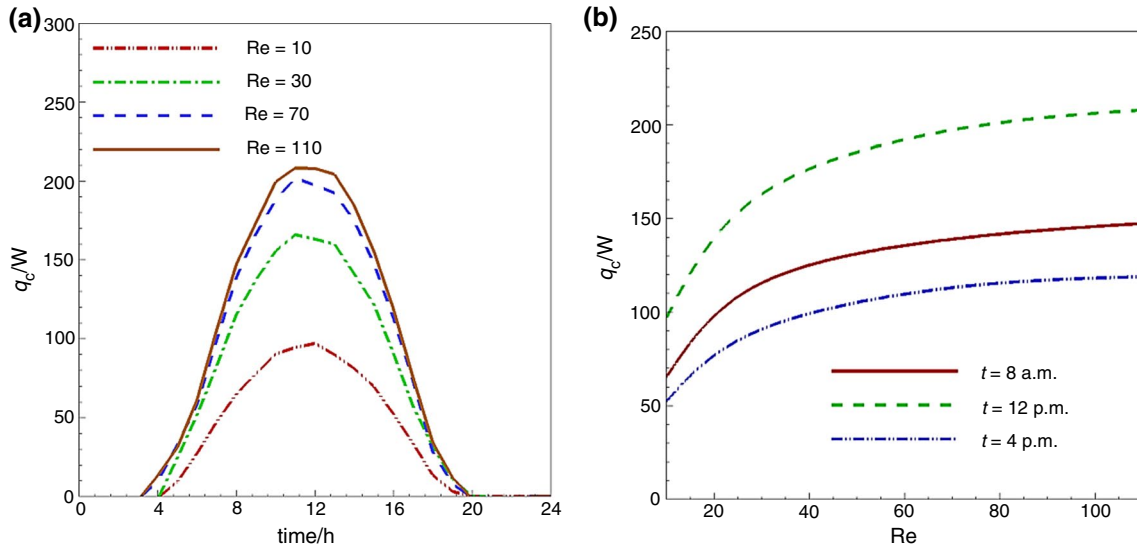
Fig. 12 **a** The thermal power received from the porous channel over the day. **b** The thermal power changes versus of Reynolds at three specified hours
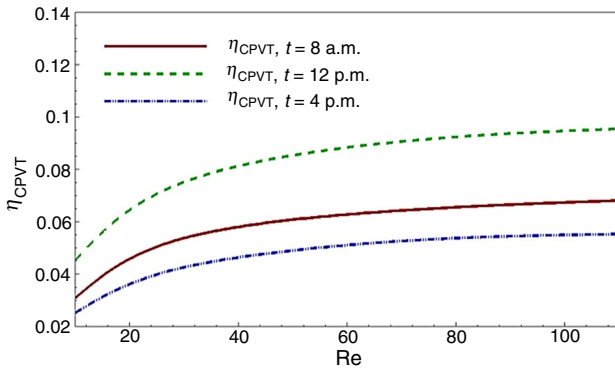

Fig. 13 The first law of thermodynamics efficiency of the concentration photovoltaic thermal (CPVT)

than other thermal photovoltaic systems mentioned in the literature.

Comparing Fig. 13 with Fig. 16, it is found that the changes in the second law efficiency is less than that of the first law efficiency and the second law of thermodynamics efficiency is greater than the first law of thermodynamics efficiency at Reynolds numbers less than 30 and 14 p.m. In general, a summary of the modeling results can be found in Table 1. According to Table 1, the mean values are expressed in terms of Reynolds number during a day at 8 a.m., 12 p.m. and 16 p.m.
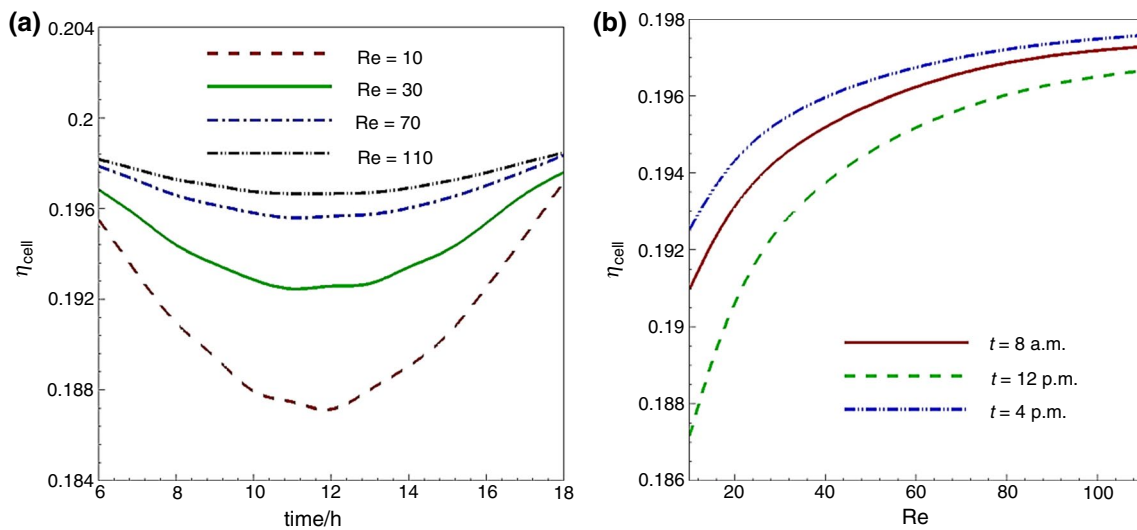

Fig. 14 **a** The variation of PV cell efficiency during the day at different Reynolds numbers. **b** The variation of PV cell efficiency versus Reynolds number
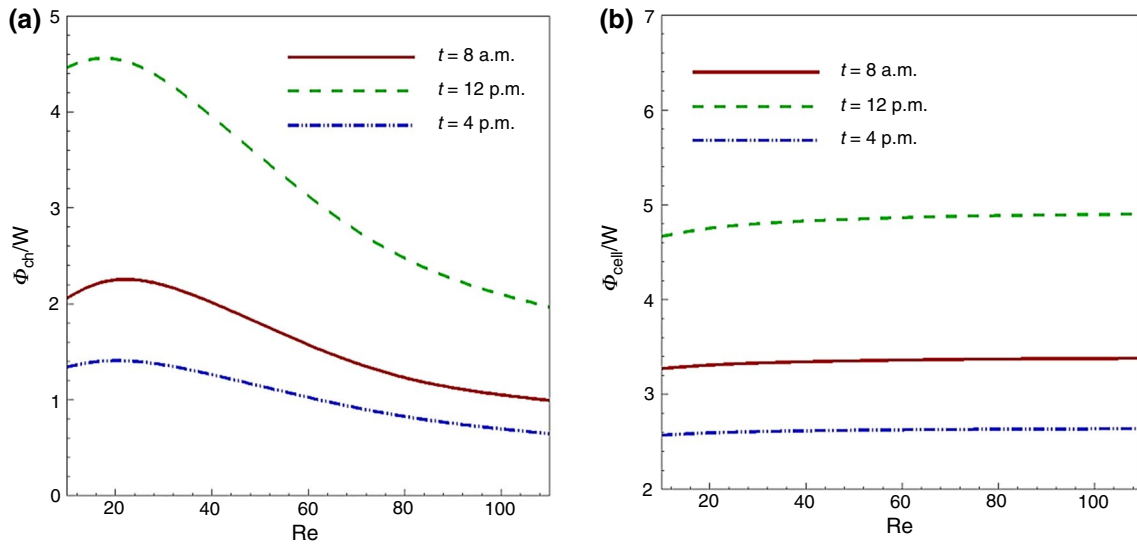
Fig. 15 **a** The variation of exergy porous channel versus Reynolds. **b** The variation of exergy PV cell versus Reynolds
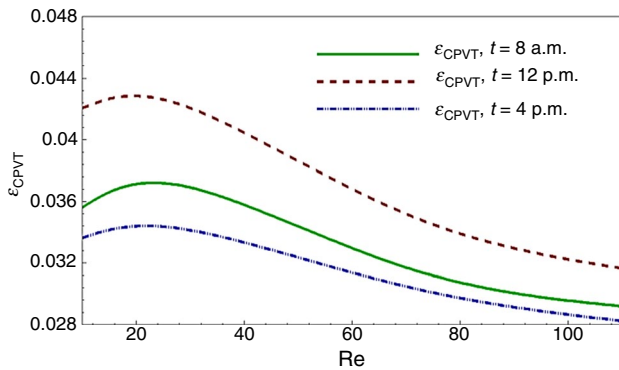

Fig. 16 The second law of thermodynamics efficiency of the concentration photovoltaic thermal (CPVT)

Table 1 The performance parameters in this study

Parameters	8 a.m.	12 p.m.	16 p.m.
η_{Cell}	0.194	0.193	0.195
η_{ch}	0.729	0.712	0.751
η_{CPVT}	0.054	0.076	0.043
η_{conc}	0.064	0.064	0.064
ϕ_{ch}	1.656	3.380	1.066
ϕ_{Cell}	3.337	4.810	2.613
ε_{CPVT}	0.033	0.037	0.031

Conclusions

In this work, energy and exergy analysis over the solar thermal photovoltaic system coupled with Al_2O_3 nanofluid flow into the porous channel is studied during a day for Mashhad city in Iran. The effects of the nanofluid flow into porous channel on the photovoltaic cell temperature and PV cell efficiency under time variable solar heat flux and the heat flux received from the parabolic dish concentrator are also discussed. Furthermore, the efficiency of the first and second law of thermodynamics is calculated. The most important results are as follows:

- The variation in temperature of the nanofluid is influenced by the porosity and permeability parameters. The rate changes in nanofluid temperature is 53.4% at 12 p.m. and Reynolds number of 10.
- The highest average nanofluid temperature is 58° C at Reynolds number of 10, while it is 32° C at Reynolds number equal to 110.
- The highest average PV cell temperature is 47 °C at 12 p.m., while at this time, the lowest average PV cell temperature is 30° C. In addition, the changes in PV cell temperature at Reynolds number less than 40 are more significant compared to Reynolds numbers greater than 80.
- With increasing Reynolds number, the first law efficiency increases due to more porous channel cooling as the highest first law efficiency is 9.5% and the lowest is 2.4%.
- The increase in PV cell efficiency with increasing Reynolds number is due to the more cooling of the nanofluid flow inside the porous channel, and the difference between the highest efficiency and the lowest value is 5% at 12 p.m.
- The second law of thermodynamics efficiency decreases as Reynolds number increases as the highest second law

of thermodynamics efficiency is 4.2% and the lowest is 2.8%.

References

1. Deymi-Dashtebayaz M, Maddah S, Goodarzi M, Maddah O. Investigation of the effect of using various HFC refrigerants in geothermal heat pump with residential heating applications. J Therm Anal Calorim. 2020. https://doi.org/10.1007/s10973-020-09539-5.

2. Ebrahimi-Moghadam A, Deymi-Dashtebayaz M, Jafari H, Niazmand A. Energetic, exergetic, environmental and economic assessment of a novel control system for indirect heaters in natural gas city gate stations. J Therm Anal Calorim. 2020;1:1–16. https://doi.org/10.1007/s10973-020-09413-4.

3. Farzaneh-Gord M, Arabkoohsar A, Deymi-Dashtebayaz M, Machado L, Koury RNN. Energy and exergy analysis of natural gas pressure reduction points equipped with solar heat and controllable heaters. Renew Energy. 2014;72:258–70. https://doi.org/10.1016/j.renene.2014.07.019.

4. Deymi-Dashtebayaz M, Tayyeban E. Multi objective optimization of using the surplus low pressure steam from natural gas refinery in the thermal desalination process. J Clean Prod. 2019;238:117945. https://doi.org/10.1016/j.jclepro.2019.117945.

5. Lovegrove K, Csiro WS. Introduction to concentrating solar power (CSP) technology. Concentrating Solar Power Technology. New York: Elsevier; 2012. p. 3–15.

6. Sharaf OZ, Orhan MF. Concentrated photovoltaic thermal (CPVT) solar collector systems: part I—fundamentals, design considerations and current technologies. Renew Sustain Energy Rev. 2015;50:1500–65. https://doi.org/10.1016/j.rser.2015.05.036.

7. Karathanassis IK, Papanicolaou E, Belessiotis V, Bergeles GC. Design and experimental evaluation of a parabolic-trough concentrating photovoltaic/thermal (CPVT) system with highefficiency cooling. Renew Energy. 2017;101:467–83. https://doi.org/10.1016/j.renene.2016.09.013.

8. Wang G, Chen Z, Hu P. Design and experimental investigation of a Multi-segment plate concentrated photovoltaic solar energy system. Appl Therm Eng. 2017;116:147–52. https://doi.org/10.1016/j.applthermaleng.2017.01.045.

9. Ma X, Zheng H, Chen Z. An investigation on a compound cylindrical solar concentrator (CCSC). Appl Therm Eng. 2017. https://doi.org/10.1016/j.applthermaleng.2017.04.030.

10. Shadmehri M, Narei H, Ghasempoura R, Shafii MB. Numerical simulation of a concentrating photovoltaic-thermal solar system combined with thermoelectric modules by coupling Finite Volume and Monte Carlo Ray-Tracing methods. Energy Convers Manag. 2018;172:343–56. https://doi.org/10.1016/j.enconman.2018.07.034.

11. Alizadeh H, Ghasempour R, Shafii MB, Ahmadi MH, Yan W-M, Nazari MA. Numerical simulation of PV cooling by using single turn pulsating heat pipe. Int J Heat Mass Transf. 2018;127:203–8. https://doi.org/10.1016/j.ijheatmasstransfer.2018.06.108.

12. Kandilli C, Külahlı G. Performance analysis of a concentrated solar energy for lightingpower generation combined system based on spectral beam splitting. Renew Energy. 2017;101:713–27. https://doi.org/10.1016/j.renene.2016.09.032.

13. Kandilli C. Performance analysis of a novel concentrating photovoltaic combined system. Energy Convers Manag. 2013;67:186–96. https://doi.org/10.1016/j.enconman.2012.11.020.

14. Sanaye S, Sarrafi A. Optimization of combined cooling, heating and power generation by a solar system. Renew Energy. 2015;80:699–712. https://doi.org/10.1016/j.renene.2015.02.043.

15. Ferchichi S, Kessentini H, Morales-Ruiz S, Rigola J, Bouden C, Olivab A. Thermal and fluid dynamic analysis of Direct Steam Generation Parabolic Trough Collectors. Energy Convers Manag. 2019;196:467–83. https://doi.org/10.1016/j.enconman.2019.05.107.

16. Günther M, Shahbazfar R. Solar dish technology. Chapter 7, Advanced CSP teaching materials. Enermena. 2018;1–63.

17. Moraveji MK, Darabi M, Haddad SMH, Davarnejad R. Modeling of convective heat transfer of a nanofluid in the developing region of tube flow with computational fluid dynamics. Int Commun Heat Mass Transf. 2011;38:1291–5. https://doi.org/10.1016/j.icheatmasstransfer.2011.06.011.

18. Deymi-Dashtebayaz M, Akhoundi M, Ebrahimi-Moghadam A, Moghadam AJ, Arabkoohsar A, Farzaneh-Gord M. Thermohydraulic analysis and optimization of CuO/water nanofluid inside helically dimpled heat exchangers. J Therm Anal Calorim. 2020;1:1–16. https://doi.org/10.1007/s10973-020-09398-0.

19. Xu Z, Kleinstreuer C. Concentration photovoltaic–thermal energy co-generation system using nanofluids for cooling and heating. Energy Convers Manag. 2014;87:504–12. https://doi.org/10.1016/j.enconman.2014.07.047.

20. Fayaz H, Nasrina R, Rahim NA, Hasanuzzamana M. Energy and exergy analysis of the PVT system: Effect of nanofluid flow rate. Solar Energy. 2018;169:217–30. https://doi.org/10.1016/j.solener.2018.05.004.

21. Okonkwo EC, Essien EA, Akhayere E, Abid M, Kavaz D, Ratlamwal TAH. Thermal performance analysis of a parabolic trough collector using waterbased green-synthesized nanofluids. Sol Energy. 2018;170:658–70. https://doi.org/10.1016/j.solener.2018.06.012.

22. An W, Li J, Ni J, Taylor RA, Zhu T. Analysis of a temperature dependent optical window for nanofluid-based spectral splitting in PV/T power generation applications. Energy Convers Manag. 2017;151:23–31. https://doi.org/10.1016/j.enconman.2017.08.080.

23. Mousa OB, Taylor RA, Shirazi A. Multi-objective optimization of solar photovoltaic and solar thermal collectors for industrial rooftop applications. Energy Convers Manag. 2019;195:392–408. https://doi.org/10.1016/j.enconman.2019.05.012.

24. Fanaee SA, Rezapour M. The modeling of constant/variable solar heat flux into a porous coil with concentrator. J Solar Energy Eng (ASME). 2020;142(1):9. https://doi.org/10.1115/1.4044126.

25. Radwan A, Ahmed M, Ookawara S. Performance enhancement of concentrated photovoltaic systems using a microchannel heat sink with nanofluids. Energy Convers Manag. 2016;119:289–303. https://doi.org/10.1016/j.enconman.2016.04.045.

26. Alobaida M, Hughesa B, Calautitb JK, O'Connora D, Heyes A. A review of solar driven absorption cooling with photovoltaic thermal systems. Renew Sustain Energy Rev. 2017;76:728–42. https://doi.org/10.1016/j.rser.2017.03.081.

27. Abdallah SR, Saidani-Scott H, Abdellatif OE. Performance analysis for hybrid PV/T system using low concentration MWCNT (water-based) nanofluid. Solar Energy. 2019;181:108–15. https://doi.org/10.1016/j.solener.2019.01.088.

28. Hader M, Al-Kouz W. Performance of a hybrid photovoltaic/thermal system utilizing water-Al$_2$O$_3$ nanofluid and fins. Int J Energy Res. 2019;43:219–30. https://doi.org/10.1002/er.4253.

29. Cummins BM, Chinthapatla R, Ligler FS, Walker GM. Time-dependent model for fluid flow in porous materials with multiple pore sizes. Anal Chem. 2017;89(8):4377–81. https://doi.org/10.1021/acs.analchem.6b04717.

30. Diersch H-JG. Finite element modeling of flow, mass and heat transport in porous and fractured media. Berlin: Springer; 2014.

31. Furman EL, Finkelstein AB, Cherny ML. Permeability of aluminium foams produced by replication casting. Metals. 2013;3:49–57. https://doi.org/10.3390/met3010049.

32. Bayomy AM, Saghir MZ. Heat transfer characteristics of aluminum metal foam subjected to a pulsating/steady water flow: experimental and numerical approach. Int J Heat Mass Transf. 2016;97:318–36. https://doi.org/10.1016/j.ijheatmasstransfer.2016.02.009.

33. Bayomy AM, Saghir MZ. Experimental study of using c-Al_2O_3– water nanofluid flow through aluminum foam heat sink: comparison with numerical approach. Int J Heat Mass Transf. 2017;107:181–203. https://doi.org/10.1016/j.ijheatmasstransfer.2016.11.037.

34. Dukhan N, Chen KC. Heat transfer measurements in metal foam subjected to constant heat flux. Exp Therm Fluid Sci. 2007. https://doi.org/10.1016/j.expthermflusci.2007.08.004.

35. Anoop KB, Sundararajan T, Das SK. Effect of particle size on the convective heat transfer in nanofluid in the developing region. Int J Heat Mass Transf. 2009;52:2189–95. https://doi.org/10.1016/j.ijheatmasstransfer.2007.11.063.

36. Xu H, Zhao C, Vafai K. Analytical study of flow and heat transfer in an annular porous medium subject to asymmetrical heat fluxes. Heat Mass Transf. 2017;53(8):2663–76.

37. Awin Y, Dukhan N. Experimental performance assessment of metal-foam flow fields for proton exchange membrane fuel cells. Appl Energy. 2019;252:113458. https://doi.org/10.1016/j.apenergy.2019.113458.

38. Chen X, Xia X, Sun C, Wang F, Liu R. Performance evaluation of a double-pipe heat exchanger with uniform and graded metal foams. Heat Mass Transf. 2019. https://doi.org/10.1007/s00231-019-02700-3.

39. Ghahremannezhad A, Vafai K. Thermal and hydraulic performance enhancement of microchannel heat sinks utilizing porous substrates. Int J Heat Mass Transf. 2018;122:1313–26. https://doi.org/10.1016/j.ijheatmasstransfer.2018.02.024.

40. Nield DA, Bejan A. convection in porous media. 3rd ed. New York: Springer; 2006.

41. Bellos E, Tzivanidis C. Investigation of a nanofluid-based concentrating thermal photovoltaic with a parabolic reflector. Energy Convers Manag. 2019;180:171–82. https://doi.org/10.1016/j.enconman.2018.11.008.

42. Gu Y, Zhang X, Myhren JA, Han M, Chen X, Yuan Y. Techno-economic analysis of a solar photovoltaic/thermal (PV/T) concentrator for building application in Sweden using Monte Carlo method. Energy Convers Manag. 2018;165:8–24. https://doi.org/10.1016/j.enconman.2018.03.043.

43. Bellos E, Tzivanidis C, Nikolaou N. Investigation and optimization of a solar assisted heat pump driven by nanofluid-based hybrid PV. Energy Convers Manag. 2019;198:111831. https://doi.org/10.1016/j.enconman.2019.111831.

44. Electronics L. LG305N1C-B3. In: www.lg-solar.com, www.lgsolarusa.com, editors. U.S.A. Inc2014.